Applied Physics Letters

RESEARCH ARTICLE | APRIL 30 2025

Resonant escape in Josephson tunnel junctions under millimeter-wave irradiation

J. N. Kämmerer ; S. Masis ; K. Hambardzumyan ; P. Lenhard ; U. Strobel ; J. Lisenfeld ; H. Rotzinger ; A. V. Ustinov

Appl. Phys. Lett. 126, 172602 (2025)
https://doi.org/10.1063/5.0258193

AIP Publishing

Applied Physics Letters ARTICLE pubs.aip.org/aip/apl

Resonant escape in Josephson tunnel junctions under millimeter-wave irradiation

Cite as: Appl. Phys. Lett. **126**, 172602 (2025); doi: 10.1063/5.0258193
Submitted: 15 January 2025 · Accepted: 14 April 2025 ·
Published Online: 30 April 2025

J. N. Kämmerer,[1,a)] S. Masis,[1] K. Hambardzumyan,[1] P. Lenhard,[1] U. Strobel,[1] J. Lisenfeld,[1] H. Rotzinger,[1,2] and A. V. Ustinov[1,2]

AFFILIATIONS

[1]Physikalisches Institut, Karlsruhe Institute of Technology, 76131 Karlsruhe, Germany
[2]Institute for Quantum Materials and Technology, Karlsruhe Institute of Technology, 76344 Eggenstein-Leopoldshafen, Germany

[a)]Author to whom correspondence should be addressed: jonas.kaemmerer@kit.edu

ABSTRACT

The microwave-driven dynamics of the superconducting phase difference across a Josephson junction is now widely employed in superconducting qubits and quantum circuits. With their typical energy level separation frequency being several GHz, cooling these quantum devices to the ground state requires temperatures below 100 mK. Pushing the operation frequency of superconducting qubits up may allow for operation of superconducting qubits at 1 K and even higher temperatures. Here, we present measurements of the switching currents of niobium/aluminum–aluminum oxide/niobium Josephson junctions in the presence of millimeter-wave radiation at frequencies above 100 GHz. The observed switching current distributions display clear double-peak structures, which result from the resonant escape of the Josephson phase from a stationary state. We show that the data can be well explained by the strong-driving model including the irradiation-induced suppression of the potential barrier. While still being measured in the quasi-classical regime, our results point toward a feasibility of operating phase qubits around 100 GHz.

Quantum circuits employing superconducting qubits have seen a lot of progress over the past two decades.[1] These circuits operate at microwave frequencies, typically around 4–8 GHz, and temperatures around 20 mK. Cooling is required to reduce the population of the excited states of these qubits, which translates into fulfilling the temperature condition $T \ll T_0 = hf/k_B$. Here, h is the Planck constant, f is the frequency of the transition between the ground and first excited states of the qubit, and k_B is the Boltzmann constant. For the transition frequency $f = 4$ GHz, the temperature T_0 is about 200 mK. However, it appears interesting and appealing trying to increase the qubit operation frequency to explore the possibility of operating them at temperatures much higher than currently required for superconducting quantum computers.

Increasing the qubit operation frequency beyond 20–30 GHz is hardly possible when using aluminum, which is currently the standard material for most modern quantum circuits. The superconducting gap energy of aluminum,[2] which is on the order of 0.18 meV, is equal to the energy of photons with a frequency of 87 GHz. An appropriate superconducting material for making high-frequency qubits can be niobium or niobium nitride, both having superconducting gap energies larger by an order of magnitude than aluminum. Furthermore, reaching the above goal also requires junctions with significantly higher Josephson plasma frequency, which primarily depends on the critical current density of the junctions.

In this work, we report millimeter (mm)-wave spectroscopy of the potential well profile for a current-biased Nb/Al-AlO_x/Nb junction. Similarly to the previously studied superconducting microwave phase qubit,[3–5] we measure the statistics of the escape events from the superconducting state as a function of bias current with applied electromagnetic radiation in the range of 100–110 GHz. At the chosen mm-wave radiation power level, the switching current distributions display double-peak features, which result from the resonant escape from a stationary state.[6] While the measurements here are performed at a relatively high temperature of 4.2 K in the regime of the thermally activated escape, our results validate the fabrication of low-loss Josephson tunnel junctions with high plasma frequency and demonstrate the possibility of operating Josephson phase qubits at mm-wave frequencies.

A description of the Josephson phase dynamics including the behavior at finite voltage is provided by the resistively and capacitively shunted junction (RCSJ) model.[7] This model takes into account the

dissipative quasiparticle current at finite voltage V across the Josephson junction by means of the linear shunt resistance R. The shunt capacitance C models the geometric capacitance of the junction electrodes. The effect of thermal fluctuations is taken into account by the addition of a Johnson noise current I_F, which is determined by the shunt resistance R at temperature T.[4,8,9] The dynamical behavior of the junction is described by[4]

$$C\left(\frac{\Phi_0}{2\pi}\right)^2\ddot{\delta}+\frac{1}{R}\left(\frac{\Phi_0}{2\pi}\right)^2\dot{\delta}+\frac{I_c\Phi_0}{2\pi}(\sin\delta-I/I_c)+I_F(t)=0, \quad (1)$$

where I is the total current flowing through the junction, I_c denotes the critical current of the junction, Φ_0 represents the flux quantum, and δ is the Josephson phase, i.e., the phase difference across the junction.

Equation (1) has the mechanical analog of a particle of mass $m=(\Phi_0/2\pi)^2C$ moving along a tilted-washboard potential given by[7]

$$U(\delta)=-E_J\cos\delta-\left(\frac{\Phi_0 I}{2\pi}\right)\delta, \quad (2)$$

where the phase δ is interpreted as the position and $E_J=I_c\Phi_0/(2\pi)$ denotes the Josephson energy. The curvature at the potential minima δ_m of (2) defines the frequency of small oscillations,[9]

$$\omega_0(I)=\omega_p\cdot\left[1-\left(\frac{I}{I_c}\right)^2\right]^{1/4}, \quad (3)$$

with $\omega_p=(2eI_c/\hbar C)^{1/2}$ the plasma frequency of the junction. The quality factor $Q=\omega_0RC$ describes the damping of the classical oscillatory behavior of the phase at the small oscillation frequency ω_0.[4] When the bias current surpasses I_c, the minima δ_m vanish and the particle is moving down the potential hill, which causes a finite voltage V across the junction.

For bias currents close to the critical current $(1-I/I_c)\ll 1$, the wells of the tilted-washboard potential are well approximated by a cubic potential[4,9] with barrier height $\Delta U=\left(4\sqrt{2}E_J/3\right)(1-I/I_c)^{3/2}$.

In underdamped junctions, defined in terms of the McCumber parameter $\beta_C=(\omega_pRC)^2$ as junctions with $\beta_C\gg 1$, thermal noise enables switching of the junction from the superconducting to the voltage state for bias currents $I_{sw}<I_c$.[9] This process is described by a thermally activated escape of the phase from a metastable well. Following the calculations conducted by Kramers,[10] the thermal escape rate is given by[4,11,12]

$$\Gamma_{th}=a_t\frac{\omega_0}{2\pi}\exp\left(-\frac{\Delta U}{k_BT}\right), \quad (4)$$

where ΔU denotes the barrier height and ω_0 plays the role of an attempt frequency. The damping-dependent transmission factor a_t in the regime of weak to moderate damping and in cubic approximation is given by $a_t=4a/[(1+aQk_BT/1.8\Delta U)^{1/2}+1]^2$ with a numerical constant $a\approx 1$.[13]

The crossover temperature, given by $T_{cr}=\hbar\omega_0/(2\pi k_B)$ in the weak-damping limit, separates the thermal regime, where $T\gg T_{cr}$, from the quantum regime, where $T\ll T_{cr}$, where the escape is dominated by macroscopic quantum tunneling.[4,12,14]

The escape temperature T_{esc} is related to the escape rate Γ via[4]

$$\Gamma=\frac{\omega_0}{2\pi}\exp\left(-\frac{\Delta U}{k_BT_{esc}}\right). \quad (5)$$

To a good approximation, T_{esc} is independent of the bias current and provides a measure for the escape process in addition to the bias current-dependent Γ. In the thermal regime, the escape temperature is derived from Eq. (4) as

$$T_{esc}=\frac{T}{1-\ln a_t/\left[\Delta U/(k_BT)\right]}, \quad (6)$$

which is expected to be close to the actual temperature.[4]

Making use of the cubic approximation for the potential barrier, Eq. (5) yields[4,9]

$$\Gamma=\frac{\omega_0}{2\pi}\cdot\exp\left\{\left(\frac{E_J}{k_BT_{esc}}\frac{4\sqrt{2}}{3}\right)\cdot\left(1-\frac{I}{I_c}\right)^{3/2}\right\}. \quad (7)$$

Therefore, the escape rate calculated from the measured switching current statistics in the thermal regime depends on three parameters: I_c, T_{esc}, and ω_p.

The irradiation of microwaves onto a Josephson junction causes a resonant enhancement of the escape rate,[3–6,15,16] which has been observed in measurements of the switching current distribution below[3,5] as well as above[15] the crossover temperature T_{cr}. This microwave-induced rate enhancement results in a multi-peaked switching current distribution and the resonant peak position is dependent on the irradiation frequency, in good agreement with the frequency of small oscillations $\omega_0(I)$.[5,15]

A quantum model for the escape in the strong-driving limit[6] describes both the quantum and the thermal regimes. In the presence of microwave irradiation at a frequency $\omega/(2\pi)$ and power P, the escape mechanism of the phase in the limit of strong driving, defined by $(\omega/\omega_p)^5\gg\hbar\omega_p/E_J$, is governed by a process of effective barrier suppression. By taking into account thermal fluctuations, the average shift in switching current $\langle\delta I_{sw}(P)\rangle=1-\langle I_{sw}(P)\rangle/I_c$ is described by a transcendent equation as follows:

$$\langle\delta I_{sw}(P)\rangle=\langle\delta I_{sw}(0)\rangle+k^{-1}P\times\sum_{nm}\frac{f_{nm}^4}{\left[\hbar^{-1}E_{nm}(\langle\delta I_{sw}(P)\rangle)-\omega\right]^2+\alpha^2}. \quad (8)$$

Here, k is the microwave coupling coefficient, $\alpha=\omega/\sqrt{Q}$ is the damping parameter, $E_{nm}(I)=E_n(I)-E_m(I)$ is the separation of the resonantly interacting energy levels, and $f_{nm}=\langle n|\hat{\delta}|m\rangle$ denote the matrix elements of the phase operator. The damping parameter α is not only dependent on the quasiparticle conductance but also influenced by the frequency-dependent impedance of the junction leads.[4] For temperatures above T_{cr}, the fluctuation induced shift in a current sweep experiment with constant sweep-rate $\dot{I}$ is given by

$$\langle\delta I_{sw}(0)\rangle\approx\left[\frac{k_BT}{2E_J}\cdot\ln\left(\frac{\omega_pI_c}{2\pi\dot{I}}\right)\right]^{2/3}. \quad (9)$$

Depending on damping, temperature, and microwave power, Eq. (8) possesses multiple solutions, explaining the existence of double-peak structures in the switching current distribution.[6]

In the harmonic approximation, the sum in Eq. (8) is reduced to the term with $n = 0$, $m = 1$ and the transition frequency is approximated by the small oscillation frequency ω_0.[6,16] By utilizing the transition matrix element of the harmonic oscillator,[17] Eq. (8) simplifies to[16]

$$\langle \delta I_{sw}(P) \rangle = \langle \delta I_{sw}(0) \rangle + k^{-1} P \frac{4e^4}{\hbar^2 \omega_0^2 C^2} \times \left([\omega_0(\langle \delta I_{sw}(P) \rangle) - \omega]^2 + \frac{\omega^2}{Q} \right)^{-1}. \quad (10)$$

The investigated samples were fabricated with a Nb/Al-AlO_x/Nb trilayer process, as described elsewhere.[18] The expected critical current density is in the range of 2000–2200 A cm^{-2} at 100 mK, while the expected junction capacitance is around 80 fFμm^{-2}. This set of fabrication parameters aims for a junction plasma frequency at zero bias around $\omega_p/2\pi = 140$ GHz. The nominal junction area is $4 \times 4\,\mu m^2$.

The sample is measured in liquid helium at 4.2 K by means of a dipstick cryostat containing a dielectric waveguide. The dielectric waveguide is connected to a horn to which the sample holder is attached, allowing for the irradiation of the sample by mm-waves. Low pass and current divider filters submerged in liquid helium reduce the thermal noise from the room temperature setup.

The measurement setup is schematically shown in Fig. 1. A current ramp with constant ramp rate $\dot{I}$ is generated by a sawtooth generator attached to a voltage-controlled current source at room temperature. A pulse generator connected to the sawtooth generator restarts the ramp in an adjustable time interval Δt_{puls} and the zero-crossing of the current ramp triggers a start signal. The voltage across

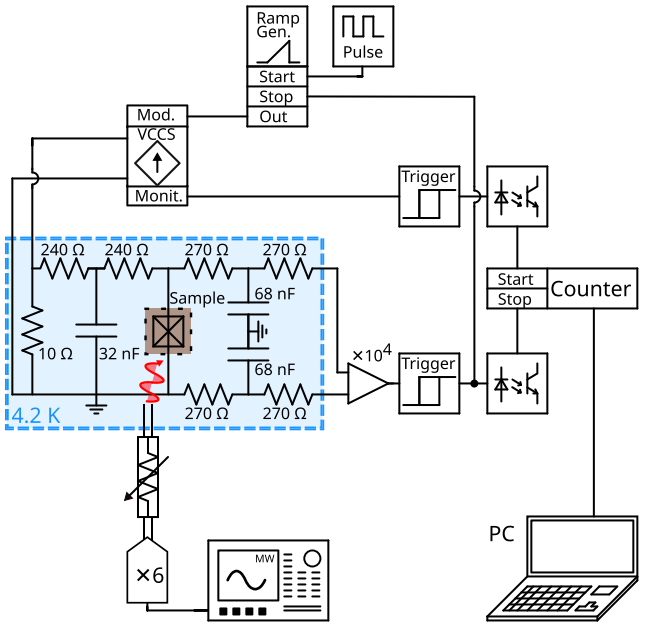

FIG. 1. Schematic of the switching current measurement setup. A time interval counter determines the duration between the zero-crossing of the bias current ramp and the moment a finite voltage develops across the junction, exceeding a threshold value. The knowledge of the current-ramp rate allows to convert the resulting time interval into a switching current. The setup allows for the irradiation of the sample by mm-waves in the frequency range 75–110 GHz.

the junction is amplified and a stop signal is triggered as soon as a threshold is exceeded. This stop signal terminates the current ramp. The interval Δt_{puls} is sufficiently large to ensure that the junction returns to the zero-voltage state.

The start and the stop signals are detected by a time interval counter *SR620* from *Stanford Research Systems* to measure the duration of the current ramp. The process is repeated continuously and the measured time intervals of the counter are read out by a computer. The time intervals are converted into switching currents through a calibration of the ramp rate.

The biasing electronic is electrically isolated from the digital data acquisition devices by optocouplers and optical fibers. Additionally, the part of the measurement setup located in liquid helium is protected by a mu-metal shield.

Electromagnetic radiation in the W-band is generated by a low-noise frequency synthesizer *APSYN140* from *AnaPico* connected to an active multiplier QMC-MX6-10F10DB from Quantum Microwave, enabling irradiation by mm-waves in the range 75–110 GHz onto the sample. The power of the mm-waves is regulated with a voltage-variable attenuator VA100-010 from Micro Harmonics. The attenuator is calibrated with the help of a vector network analyzer.

In the conducted current-ramp experiment, the junction is initially in the zero-voltage state and the bias current is increased with a constant ramp rate.[9] The probability distribution $P_{sw}(I)$ of the switching currents is defined such that the probability to measure a switching event in the small interval from I to $I + dI$ is given by $P_{sw}(I)dI$. Thus, repeatedly measuring I_{sw} allows to reconstruct $P_{sw}(I)$ from which the escape rate is calculated. The relation between $P_{sw}(I)$ and the escape rate $\Gamma(I)$ is given by[9]

$$P_{sw}(I) = \Gamma(I) \left(\frac{dI}{dt} \right)^{-1} \left(1 - \int_0^I P(\tilde{I}) d\tilde{I} \right). \quad (11)$$

For the analysis of the experimental data, the measured switching current distribution is collected in a histogram with a bin width ΔI resulting in a discrete escape probability density given by[19]

$$P_j = \frac{n_j}{N \cdot \Delta I}, \quad (12)$$

where n_j is the number of counts in the j-th bin and N is the total number of counts. The according escape rate is[4,19]

$$\Gamma(I_k) = \frac{|\dot{I}|}{\Delta I} \ln \left(\frac{\sum_{j \geq k} P_j}{\sum_{j \geq k+1} P_j} \right). \quad (13)$$

First, the switching current distribution is measured without external mm-wave irradiation. The measurement is performed with a current-ramp rate of 0.8 A s^{-1} and a measurement frequency of 200 Hz for a total of 5×10^4 counts. The result is presented in Fig. 2. The obtained asymmetric histogram with a bin width of $\Delta I \approx 58.3$ nA possesses a mean switching current of $\langle I_{sw} \rangle \approx 233.72\,\mu$A with a standard deviation of $\sigma \approx 0.62\,\mu$A. This yields a relative width of $\sigma / \langle I_{sw} \rangle \approx 2.7 \times 10^{-3}$.

A fit according to Eq. (7) with I_c, T_{esc}, and ω_p as fit parameters is performed. In this least squares fit, the weight of the data points corresponds to the square root of the number of escape events collected in

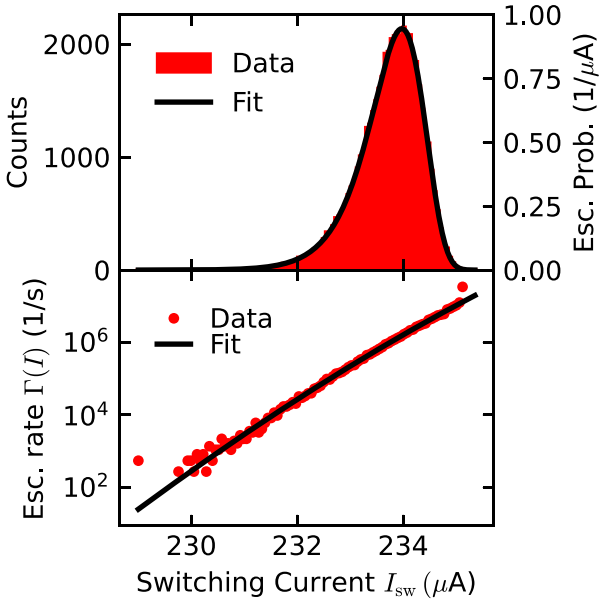

FIG. 2. Top: Switching current histogram in the thermal regime measured at 4.2 K. Bottom: The escape rate calculated from the switching current distribution. A fit of the calculated escape rate according to Eq. (7) yields $I_c = 242(1)\,\mu$A, $T_{esc} = 6.3(4)$ K, and $\omega_p/(2\pi) = 0.1$ (2) THz. The result of the fit is represented by a black curve for both the escape rate and the escape probability.

each bin.[4] This procedure does not allow for a precise determination of ω_p, but provides a value for the critical current $I_c = 242(1)\,\mu$A. The escape rates and escape probabilities calculated from the fit parameters are in agreement with the experimental data as shown in Fig. 2.

Under mm-wave irradiation, the switching current distribution, with the primary peak located at I_p, shifts to lower values with increasing mm-wave power, until a second resonant peak at position $I_r < I_p$ develops. This double-peak structure is shown in the inset of Fig. 3 for a radiation frequency of 109.92 GHz. By increasing the mm-wave power further, the primary peak vanishes and the resonant peak shifts to lower values.

The frequency of the irradiated mm-waves is varied to measure the dependence of the resonant peak position I_r on the radiation frequency. Here, the power of the irradiated mm-waves is adjusted, so the primary and the resonant peaks are of equal height. This ensures a statistically significant measurement of both peaks and provides a measure that allows to compare and reproduce the switching current measurements at varying frequencies. Each histogram is taken with at least 2×10^4 counts. The peak positions are determined by the fit of a curve with a double-Lorentzian shape for each histogram.

The results are depicted in Fig. 3. A fit of $f_0(I) = \omega_0/(2\pi)$ according to Eq. (3) to the observed data yields an estimate for ω_p. The accuracy of this heuristic approach is limited, as the resonant peak position I_r is dependent on the mm-wave power. The plasma frequency $\omega_p/(2\pi) = 138.3(7)$ GHz, extracted as a fit parameter from this spectroscopic measurements, is close to the design expectations. The corresponding maximum crossover temperature, evaluated at zero bias current, is $T_{cr} = 1.056(5)$ K, which is lower than the bath temperature of liquid helium 4.2 K. This confirms that the measurements presented in this work are performed in the thermal regime.

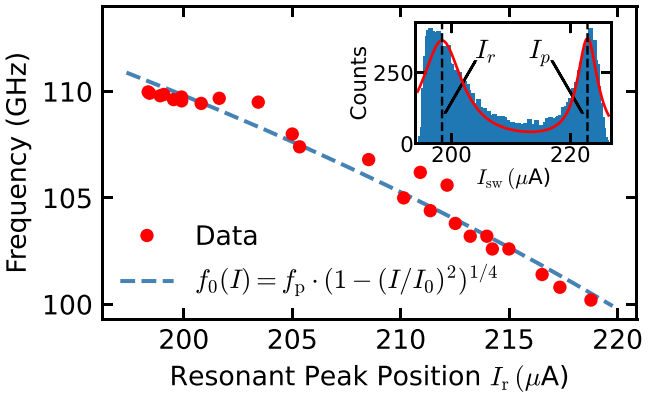

FIG. 3. Results of the spectroscopic determination of the plasma frequency. The position of the resonant peak in the switching current distribution is measured as a function of the irradiation frequency. The inset shows a switching current histogram measured under irradiation of mm-waves at 109.92 GHz and a double-Lorentzian fit, performed in order to determine the peak positions. The dashed blue line shows a fit of the frequency of small oscillations $f_0 = \omega_0/(2\pi)$ according to Eq. (3) to the observed data with the parameters $I_c = 258(3)\,\mu$A and $f_p = \omega_p/(2\pi) = 138.3(7)$ GHz.

Measurements of the switching current distribution in dependence of the irradiated mm-wave power are shown in Fig. 4 for three different frequencies. For each mm-wave power, a measurement with a total number of 2×10^4 counts is taken. It is visible how the branch of the primary peak is moving to lower switching currents for increasing mm-wave power. The development of a resonant peak is observed, which coexists with the main branch within a narrow range of mm-wave power, where the switching current distribution displays a double-peak structure as shown in the inset of Fig. 3. By further increasing the mm-wave power, the primary branch vanishes while the resonant branch becomes the main branch. In comparison, the jump between the primary and the resonant branch is less pronounced for lower frequencies. The relative width of the resonant peak, determined at a level of mm-wave power for which only the resonant peak is observed, is of the order of $\sigma/\langle I_{sw}\rangle \approx 1.8 \times 10^{-3}$. This value is smaller than the relative width of the primary peak observed in the absence of mm-wave irradiation.

Using $I_c = 242\,\mu$A, $\omega = 2\pi \cdot 100$ GHz, and $\omega_p = 2\pi \cdot 138.3$ GHz yields $E_J \cdot (\omega/\omega_p)^5/\hbar\omega_p \approx 170 \gg 1$, i.e., the condition for the strong-driving limit is fulfilled. Therefore, the data for the power dependence are compared to the model of effective barrier suppression. Differing widths for the primary and the resonant peak are explained by the theory of escape in the strong-driving limit, as the width of the primary peak is determined by thermal fluctuations while the width of the resonant peak depends on the damping of the junction.[6]

Figure 4 also displays fits of the solutions of Eq. (8) in the thermal regime to the measurement data. As fixed parameters, the critical current $I_c = 242\,\mu$A obtained from the switching current distribution in the absence of mm-wave irradiation is used, as well as the bath temperature of liquid helium $T = 4.2$ K. The fits for the three distinct frequencies of mm-wave radiation share the plasma frequency $\omega_p = 2\pi \cdot 145.5$ GHz as a common fit parameter. The obtained frequency-dependent effective quality factors are of the order of $Q \approx 90$, which we expect to be limited by quasiparticles at the temperature of 4.2 K.

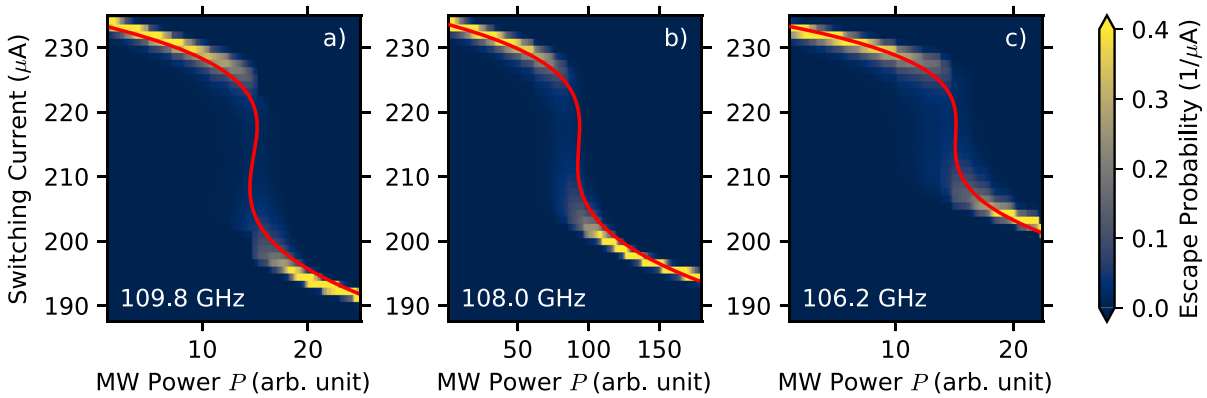

FIG. 4. Measurement of the switching current distribution in dependence of the applied mm-wave power for three different frequencies: (a) 109.8, (b) 108.0, and (c) 106.2 GHz. The red lines represent fits obtained from the solutions of Eq. (8). Fixed parameters are $I_c = 242\ \mu$A and $T = 4.2$ K. The plasma frequency $\omega_p = 2\pi \cdot 145.5$ GHz is a common fit parameter. The individual fit parameters are (a) $Q \approx 97$, $k^{-1}C^{-2} = 0.82 \times 10^{50}$ (arb. unit), (b) $Q \approx 91$, $k^{-1}C^{-2} = 0.115 \times 10^{50}$ (arb. unit), and (c) $Q \approx 90$, $k^{-1}C^{-2} = 0.6 \times 10^{50}$ (arb. unit).

In summary, we studied the interaction of Nb/Al-AlO_x/Nb Josephson tunnel junction with mm-waves by investigating the switching current distribution. The analysis of the observed double-peak structures allows for direct determination of the plasma frequency. Spectroscopic measurements of the dependence of the resonant peak bias current position on the radiation frequency are conducted. Furthermore, the dependence of the switching current distribution on the mm-wave power at fixed frequency was analyzed by means of a quantum model in the strong-driving limit. These measurements yield similar results and show that junctions with plasma frequencies of the order of $\omega_p = 2\pi \cdot 140$ GHz have been fabricated. The application of these techniques provides a quick turnaround methodology for the characterization of mm-wave Josephson junctions, allowing a rapid process development for qubit devices.

We thank T. Zwick for fruitful discussions. This work was supported by funding from the European Research Council (ERC) under the European Union's Horizon 2020 Research and Innovation Programme (project *Milli-Q*, Grant Agreement No. 101054327).

AUTHOR DECLARATIONS

Conflict of Interest

The authors have no conflicts to disclose.

Author Contributions

All authors contributed equally to the work.

J. N. Kämmerer: Writing – original draft (equal); Writing – review & editing (equal). **S. Masis:** Writing – original draft (equal); Writing – review & editing (equal). **K. Hambardzumyan:** Writing – original draft (equal); Writing – review & editing (equal). **P. Lenhard:** Writing – original draft (equal); Writing – review & editing (equal). **U. Strobel:** Writing – original draft (equal); Writing – review & editing (equal). **J. Lisenfeld:** Writing – original draft (equal); Writing – review & editing (equal). **H. Rotzinger:** Writing – original draft (equal); Writing – review & editing (equal). **A. V. Ustinov:** Writing – original draft (equal); Writing – review & editing (equal).

DATA AVAILABILITY

The data that support the findings of this study are available from the corresponding author upon reasonable request.

REFERENCES

[1]M. Kjaergaard, M. E. Schwartz, J. Braumüller, P. Krantz, J. I.-J. Wang, S. Gustavsson, and W. D. Oliver, "Superconducting qubits: Current state of play," Annu. Rev. Condens. Matter Phys. **11**, 369–395 (2020).
[2]B. W. Roberts, "Survey of superconductive materials and critical evaluation of selected properties," J. Phys. Chem. Ref. Data **5**, 581–822 (1976).
[3]J. M. Martinis, M. H. Devoret, and J. Clarke, "Energy-level quantization in the zero-voltage state of a current-biased Josephson junction," Phys. Rev. Lett. **55**, 1543–1546 (1985).
[4]J. M. Martinis, M. H. Devoret, and J. Clarke, "Experimental tests for the quantum behavior of a macroscopic degree of freedom: The phase difference across a Josephson junction," Phys. Rev. B **35**, 4682–4698 (1987).
[5]A. Wallraff, T. Duty, A. Lukashenko, and A. V. Ustinov, "Multiphoton transitions between energy levels in a current-biased Josephson tunnel junction," Phys. Rev. Lett. **90**, 037003 (2003).
[6]M. V. Fistul, A. Wallraff, and A. V. Ustinov, "Quantum escape of the phase in a strongly driven Josephson junction," Phys. Rev. B **68**, 060504 (2003).
[7]M. Tinkham, *Introduction to Superconductivity*, Dover Books on Physics, 2nd ed. (Dover Publications, Mineola, NY, 2004).
[8]V. Ambegaokar and B. I. Halperin, "Voltage due to thermal noise in the dc Josephson effect," Phys. Rev. Lett. **22**, 1364–1366 (1969).
[9]T. A. Fulton and L. N. Dunkleberger, "Lifetime of the zero-voltage state in Josephson tunnel junctions," Phys. Rev. B **9**, 4760–4768 (1974).
[10]H. A. Kramers, "Brownian motion in a field of force and the diffusion model of chemical reactions," Physica **7**, 284–304 (1940).
[11]U. Weiss, *Quantum Dissipative Systems*, Series in Modern Condensed Matter Physics No. 10, 2nd ed. (World Scientific, Singapore, River Edge, NJ, 1999).
[12]H. Grabert, P. Olschowski, and U. Weiss, "Quantum decay rates for dissipative systems at finite temperatures," Phys. Rev. B **36**, 1931–1951 (1987).
[13]M. Büttiker, E. P. Harris, and R. Landauer, "Thermal activation in extremely underdamped Josephson-junction circuits," Phys. Rev. B **28**, 1268–1275 (1983).
[14]H. Grabert and U. Weiss, "Crossover from thermal hopping to quantum tunneling," Phys. Rev. Lett. **53**, 1787–1790 (1984).
[15]N. Grønbech-Jensen, M. G. Castellano, F. Chiarello, M. Cirillo, C. Cosmelli, L. V. Filippenko, R. Russo, and G. Torrioli, "Microwave-induced thermal escape in Josephson junctions," Phys. Rev. Lett. **93**, 107002 (2004).

[16]H. F. Yu, X. B. Zhu, J. K. Ren, Z. H. Peng, D. J. Cui, H. Deng, W. H. Cao, Y. Tian, G. H. Chen, D. N. Zheng, X. N. Jing, L. Lu, and S. P. Zhao, "Resonant phase escape in $Bi_2Sr_2CaCu_2O_{8+\delta}$ surface intrinsic Josephson junctions," New J. Phys. **15**, 095006 (2013).
[17]J. M. Martinis, S. Nam, J. Aumentado, K. M. Lang, and C. Urbina, "Decoherence of a superconducting qubit due to bias noise," Phys. Rev. B **67**, 094510 (2003).
[18]U. Strobel, L. Radtke, L. Kamps, J. Voss, J. Lisenfeld, H. Rotzinger, and A. V. Ustinov, "High quality Josephson junction for mm-wave applications" (unpublished).
[19]A. Wallraff, *Fluxon Dynamics in Annular Josephson Junctions: From Relativistic Strings to Quantum Particles*, Mesoscopic Structures and Superconductivity No. 1 (Lehrstuhl für Mikrocharakterisierung, Friedrich-Alexander-University, Erlangen, 2001).